Plasma Simulations for the Assessment of Pole Erosion in the Magnetically Shielded Miniature Hall Thruster (MaSMi)

IEPC-2019-281

Presented at the 36th International Electric Propulsion Conference
University of Vienna • Vienna, Austria
September 15-20, 2019

Alejandro Lopez Ortega[1], Ioannis G. Mikellides[2], Ryan Conversano[3], Robert B. Lobbia[4] and Vernon H. Chaplin[5]
Jet Propulsion Laboratory, California Institute of Technology, Pasadena, CA, 91109, United States

Abstract: Numerical simulations have been conducted to assess the erosion rates at the pole covers of the magnetically shielded miniature (MaSMi) Hall thruster. MaSMi is part of the Ascendant Sub-kW Transcelestial Electric Propulsion System (ASTRAEUS), whose design requirements demand a xenon throughput of 100 kg, thus enabling deep space missions using SmallSats. The results of our simulations show that the proposed thickness of the graphite pole covers will not be completely eroded at end of life. We find that the erosion rates are larger near the corners of the covers, which are directly exposed to the plasma in the acceleration channel. The predicted erosion rates in these locations are close to the maximum allowable erosion rate that will prevent complete erosion before the throughput requirement for the system is fulfilled. Although we predict that the erosion rates will decrease as the corners erode, this assertion must be proven in future work. Finally, the Inconel fasteners that attach the cover to the thruster erode at a rate that is ten times larger than the surface of the pole cover, which is made of graphite. We found that a pole cover design that features a wedge for shielding the fastener barely lowers the erosion rates of the fastener to acceptable values. To further mitigate this risk, the installation of graphite covers over all of the pole-cover fasteners is proposed.

I. Introduction

The Jet Propulsion Laboratory's (JPL) Ascendant Sub-kW Transcelestial Electric Propulsion System (ASTRAEUS) program aims to enable high delta-V interplanetary exploration using SmallSat spacecraft (wet mass spanning from several 10's to 100's of kg) [1]. Numerous recent mission studies have focused on the use of SmallSats targeting both the inner solar system (Venus, Mars) [2-3] and the outer solar system (Saturn, Neptune, Uranus) [4]. ASTRAEUS is a fully integrated electric propulsion system based around the MaSMi (Magnetically Shielded Miniature) Hall thruster, which has a well-documented development history since its inception in 2011[5-14] and is the world's highest-performing sub-kW Hall thruster [15]. MaSMi achieves exceptionally high throughput capabilities through the application of magnetic shielding [16], a technique that, acknowledging that the main cause of erosion in the discharge channel is the existence of plasma potential gradients and high electron temperatures that drive energetic ions towards the walls, proposes a design strategy for the magnetic field topology that avoids such conditions. This technique has already been implemented in multiple thrusters, including the 12.5-kW Hall Effect

[1]Member of the Technical Staff, Electric Propulsion Group, 4800 Oak Grove Drive, Pasadena, CA, 91109, Mail Stop 125-109
[2]Principal Engineer, Electric Propulsion Group, 4800 Oak Grove Drive, Pasadena, CA, 91109, Mail Stop 125-109
[3]Member of the Technical Staff, Electric Propulsion Group, 4800 Oak Grove Drive, Pasadena, CA, 91109, Mail Stop 125-109
[4]Member of the Technical Staff, Electric Propulsion Group, 4800 Oak Grove Drive, Pasadena, CA, 91109, Mail Stop 125-109
[5]Member of the Technical Staff, Electric Propulsion Group, 4800 Oak Grove Drive, Pasadena, CA, 91109, Mail Stop 125-109

Rocket with Magnetic Shielding (HERMeS) program, now part of the Advanced Electric Propulsion System (AEPS) [17-19].

The physics of magnetic shielding were first described by the Jet Propulsion Laboratory (JPL) after Aerojet Rocketdyne's XR-5 (formerly the BPT-4000) reached a zero-erosion state 5.6 kh into a 10.4 kh wear test [16, 20]. Subsequently, magnetic shielding was shown by JPL to reduce erosion rates at the acceleration channel walls by three orders of magnitude in a series of simulations and experiments designed to validate the physics of magnetic shielding through modification of the H6 Hall thruster [21-23]. However, sputtering of the magnetic poles was revealed when a post-test visual inspection showed roughening of the inner and outer pole surfaces at the end of a 150-hour wear that was part of the proof of concept. Significant sputtering of the magnetic poles has rarely been observed in unshielded thrusters unless their discharge chambers are highly eroded. A second 150-hour wear test was then carried out [24] to quantify the erosion rates at the poles. Results of the second test suggested that the sputtering of the cover surface was produced by ions of relatively high energy, approximately 150 V (with an approximately 100-V margin of error due to uncertainty in the sputtering yield at that range of ion energies). The measured erosion rates were one to two orders of magnitude lower than those typically observed at the surfaces of the acceleration channel of comparable unshielded thrusters. Thus, erosion of the poles can be prevented by installing graphite pole covers with thicknesses on the order of a few millimeters. The experimental study was complemented with numerical simulations using Hall2De [25] with the help of additional measurements, which included laser-induced fluorescence measurements of the ion velocity distribution in the acceleration channel. The numerical investigation concluded that the erosion of the poles observed in the H6MS was a result of the acceleration region moving downstream of the acceleration channel, which in turn is a consequence of a shift in the location of the maximum magnetic field along the channel centerline that occurs when magnetic shielding is implemented. When the acceleration region moves downstream, the plasma potential contours at the edges of the channel allow for high energy ions to be accelerated radially towards the pole surfaces.

More recently, wear tests were performed for HERMeS at operating conditions spanning its entire operational envelope [26]. Results of the wear tests show rates of sputtering at the inner pole covers that are comparable to those found in the H6MS, with one operating condition (300 V – 20.8 A) exhibiting slightly larger (by approximately a factor of two) sputtering rates than the others. These wear tests were also complemented with Hall2De simulations [27]. Numerical results showed two distinct trends depending on the presence of large global oscillations. At large discharge voltages, the discharge current response is dominated by large oscillations with peak-to-peak amplitudes of approximately 40% of the nominal current. These oscillations move the location of maximum acceleration of ions back and forth, a mechanism that had been previously identified as a contributor to increased erosion rates in [28]. At low discharge voltages, large discharge current oscillations are not present but the location of maximum acceleration of the plasma moves downstream, increasing the erosion rates at the poles due to a larger beam divergence.

In this paper, we present a numerical investigation of the expected erosion rates at the poles of the MaSMi thruster at three conditions representative of extremes in the operational envelope (500 V – 2 A, 400 V - 2 A, and 200 V – 1 A). In Section II, we include a brief description of Hall2De and the sputtering models used to compute erosion rates from the computed plasma properties. Results of the simulations are shown in Section III. In Section IV, we compare the predicted erosion rates with measurements from the wear test [29] and discuss the salient differences in erosion patterns observed between the miniature thruster and high-power thrusters such as HERMeS and H6MS. Concluding remarks are provided in Section V.

II. Computational method

Hall2De is a 2-D axisymmetric code for the simulation of the plasma discharge in Hall thrusters whose development began about a decade ago. Specifics of the numerical implementation can be found in [30-31]. Hall2De employs a quadrilateral-based computational grid aligned with the magnetic field. The simulation domain for the MaSMi simulations comprises the acceleration channel and a region of the plume that extends several times the length of the channel in the radial and axial directions (Fig. 1), extending up to the thruster centerline where the cathode is located. The equations of motion are solved in the radial and axial directions (r-z), assuming axial symmetry along the thruster centerline.

The motion of each of the species in the plasma is solved separately. The density and velocity field of neutral particles is modeled assuming free-molecular flow, using a view-factor algorithm described in [32]. For modeling the ion population, we follow the approach first introduced in [25], where we made use of a hybrid hydrodynamics and particle-in-cell (PIC) approach for tracking the multiple ion populations present in the plasma according to their energy. This approach was motivated by the fact that pole erosion, contrary to channel erosion, can be caused by a distribution of ions with a wide variety of energy values. Ions that originate in the acceleration channel are always modeled using hydrodynamics equations since, as it was shown in [30-31], these ions have sufficiently long residence time compared to their collision time to warrant a Maxwellian distribution. The second ion population comprises ions generated in the vicinity of the cathode exit. Separate continuity and momentum equations are solved for each fluid population, *iF*, and each charge state, *iC*. Ions of different *iF* and *iC* numbers can interact with one another through ionization, charge exchange, and elastic collisions. Ions generated in the vicinity of the maximum electric field or downstream of it do not have sufficient residence time to equilibrate with the beam ions or among themselves. These ions are modeled using the PIC method. Electron motion is modeled using a fluid approach where inertia is neglected. This approach results in a vector form of Ohm's law that is solved in the directions parallel and perpendicular to the magnetic field lines and enables computation of the plasma potential when combined with current conservation and the assumption of plasma quasi-neutrality. Electron temperature is determined as the solution of an energy conservation equation.

Boundary conditions are imposed as follows. The channel walls are modeled as boron nitride insulators and the sheath that develops is computed based on the Hobbs and Wesson solution to the 1-D sheath equations [33], accounting for secondary electron emission. The anode walls and pole cover surfaces are modeled as conductors at fixed voltage. We also specify the neutral flow rate across the injection area of the anode. At the cathode boundary, we specify electron temperature, plasma potential and mass flow rate of neutrals and ions.

The erosion model in Hall2De is described in detail in [25]. Succinctly, we compute at each time-step of the simulation the erosion produced by each ion population (including PIC) as a function of the ion current density and velocity vector near the walls. The total erosion rate at each location is computed as the aggregate of the contributions to the erosion of all the ion populations divided by the simulation time. The sputtering yield is modeled as the product of the angular yield (i.e., the effect of the angle of incidence for fixed kinetic energy) and the energy yield, which depends only on the ion kinetic energy. Because ions must traverse a sheath before striking the wall, the total energy is the sum of the kinetic energy ions have acquired in the plasma upon entrance to the sheath, and the sheath potential energy. For the latter, we make use of the potential energy, transformed to ion kinetic energy as the plasma ions accelerate inside the sheath towards the solid material [33]. The angular dependence implemented in Hall2De is described in [25]. The energy yield follows a data fit to the data reported by Doerner et al [34], Rosenberg and Wehner [35], and Kolasinski [36].

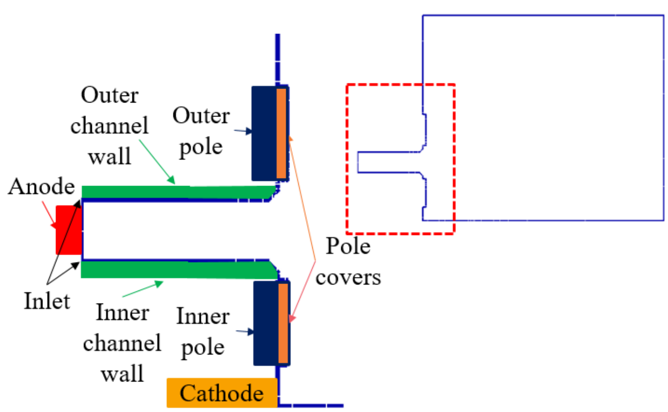

Fig. 1: Hall2De computational domain for MaSMi and schematic of the thruster geometry

III. Numerical simulation results and validation

A. Operating conditions and input parameters

MaSMi is designed to be the basis of a sub-kW electric propulsion system. The thruster has been characterized [1] for a discharge power range between 150 and 1000 W and discharge voltages between 200 and 500 V. For each operating condition, the magnetic field strength is optimized for optimum performance and/or to maintain low oscillation levels. We selected three operating conditions within the envelope of characterized conditions for this investigation (Table I). The 500 V – 2 A condition is selected as it represents the power limit of the Power Processing Unit being developed for MaSMi. The 400 V – 2 A condition is chosen in order to draw conclusions on the effect of changes in discharge voltage while keeping the discharge current constant (similar to the HERMeS investigation reported in [27], where the operating envelope between 300 and 600 V was investigated at a constant discharge current of 20.8 A) or in case the PPU has to be limited to operate below 800 V. Finally, we include the low-power condition of 200 V – 1A. This operating condition exhibits the largest oscillations, with a peak-to-peak amplitude of approximately 105% of the nominal discharge current. As observed in numerical simulations of HERMeS [27], the presence of large discharge current oscillations can adversely affect the erosion rates at the pole cover surfaces, increasing them by more than an order of magnitude.

Table I. Performance summary for MaSMi simulations

Discharge power (kW)	Discharge voltage (V)	Discharge current (A)	Anode mass flow rate (mg/s)	Cathode flow rate (% of anode flow rate)	Thrust (mN)		Peak-to-peak amplitude (% nominal current)	Oscillation frequency (kHz)
					Measured	Simulation		
1.0	500	2.0	2.58	7	14.1	11.8	30.0	20.5
0.8	400	2.0	2.51	7	47.6	44.3	30.0	20.7
0.2	200	1.0	1.29	7	54.5	52.3	106.0	25.4

A first-principles closure model for the anomalous transport of electrons across magnetic field lines in Hall thrusters remains elusive today. Thus, the anomalous collision frequency distribution in the MaSMi simulations is determined with guidance from measurements. These include performance comparisons (i.e., discharge current, thrust) as well as spatially-resolved local plasma parameters including electron temperature and ion velocity. For this study, we adopted the spatial evolution of the ion drift velocity along channel centerline as the primary measurement for informing the anomalous collision frequency in Hall2De. We employed a non-resonant laser induced fluorescence diagnostic to characterize this plasma property [37-38]. In brief, this non-resonant LIF scheme relies on inducing a transition in a metastable state of singly charged xenon ions with injected light from a tunable diode laser. By scanning the laser wavelength across this metastable transition and monitoring the intensity of the fluoresced signal, it is possible to infer the Doppler broadening in this transition state that is the result of ion motion. This in turn leads to an assessment of the local ion velocity distribution function (IVDF). The system we employed for this work yielded IVDFs with a spatial resolution of 2 mm. The values for ion velocity reported here were found by taking the first moments of the measured IVDFs. Further information about the measurements can be found in a companion paper [39]. After we determine an anomalous collision frequency distribution that yields computed results agreeing well with the experimental ion velocity along the centerline, we make other comparisons (for instance, the measured and computed thrust and the ion velocity distribution away from the channel centerline) to validate our numerical results.

Figure 2 depicts a direct comparison of the ion velocity between the simulations and the LIF measurements at the channel centerline. L is the acceleration channel length, with z/L=0 and z/L=1 at the anode and channel exit, respectively. We also present the anomalous collision frequency profiles that were employed in the simulations. The simulation results are in excellent agreement with the experiments. One important difference between these results and those found in order thrusters, such as HERMeS, is that the acceleration region does not significantly move as a function of discharge voltage. On the contrary, we found for HERMeS [27] that the acceleration region moved upstream significantly with increasing discharge voltage. In the H6MS [25], the location of the acceleration region was found to be further downstream with respect to the channel exit plane. We must emphasize that the physical mechanisms that dictate the location of the acceleration region are closely linked to the anomalous transport physics which remain elusive today [40, 41 and references therein] and, are therefore beyond the scope of this article. Another interesting feature is that the anomalous collision frequency that is required at the 200 V – 1 A condition is more than an order of magnitude larger than at the other two operating conditions inside the acceleration channel, suggesting that anomalous transport becomes more prominent as the discharge current and voltage decreases. It has been proposed [42] that in thrusters exhibiting large plasma oscillations in the kilohertz range, the amount of anomalous electron transport may also be oscillatory. In our simulations, we fix our anomalous collision frequency in time. However, the simulations with a fixed anomalous collision frequency profile did not produce the oscillation in the discharge current (~50% of nominal current) found in the experiments. The latter suggests than time-dependent anomalous transport may indeed be present in highly oscillatory cases. We thus included an oscillation in time with a frequency of 25.4 kHz (Table I) in the anomalous collision frequency for the 200 V – 1 A case in order to account for the effect of the oscillations on the erosion rate of the pole covers.

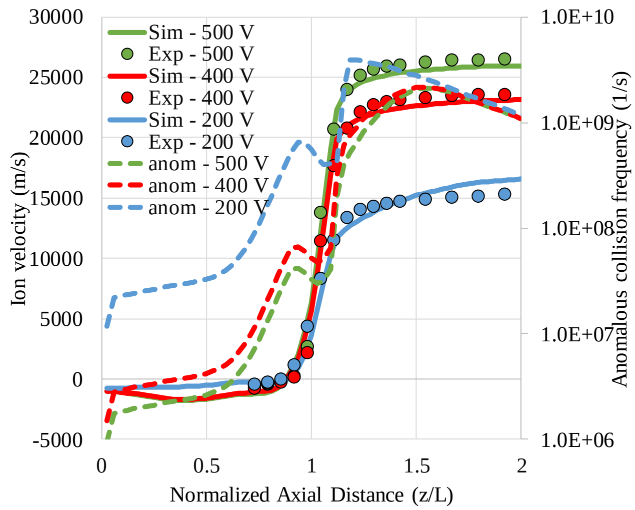

Fig. 2: Comparison between ion velocity at the channel centerline from simulations and LIF measurements for operating conditions in Table I. Anomalous collision frequency distribution employed in the simulation depicted in dashed lines.

We conclude this subsection, by providing additional comparisons between the simulations and laboratory data. In Fig. 3, we show the computed evolution of discharge current and thrust in time, which compares well to the experimental values of Table I. In Fig. 4, we depict the two-dimensional LIF measurements obtained for the 500 V – 2 A and 200 V – 1 A conditions superimposed with ion velocity streamlines extracted from the corresponding simulation. We observe that the agreement in both direction and magnitude is excellent. We found that the simulation results at the intermediate operating condition (400 V – 2 A) displays a similar level of agreement with the measurements.

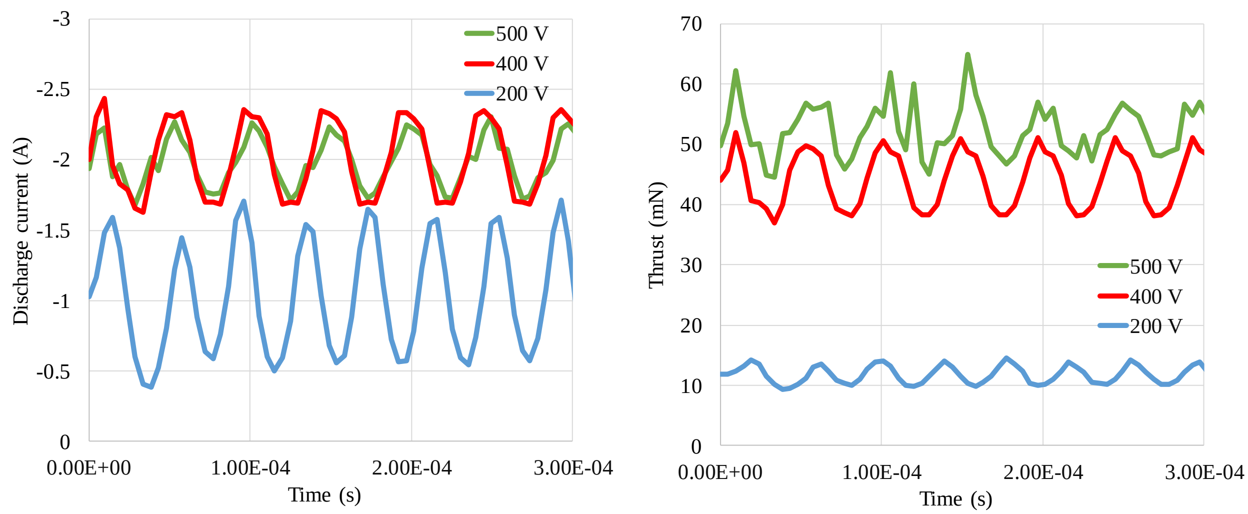

Fig. 3: Discharge current and thrust as a function of time for the three operating conditions in Table I

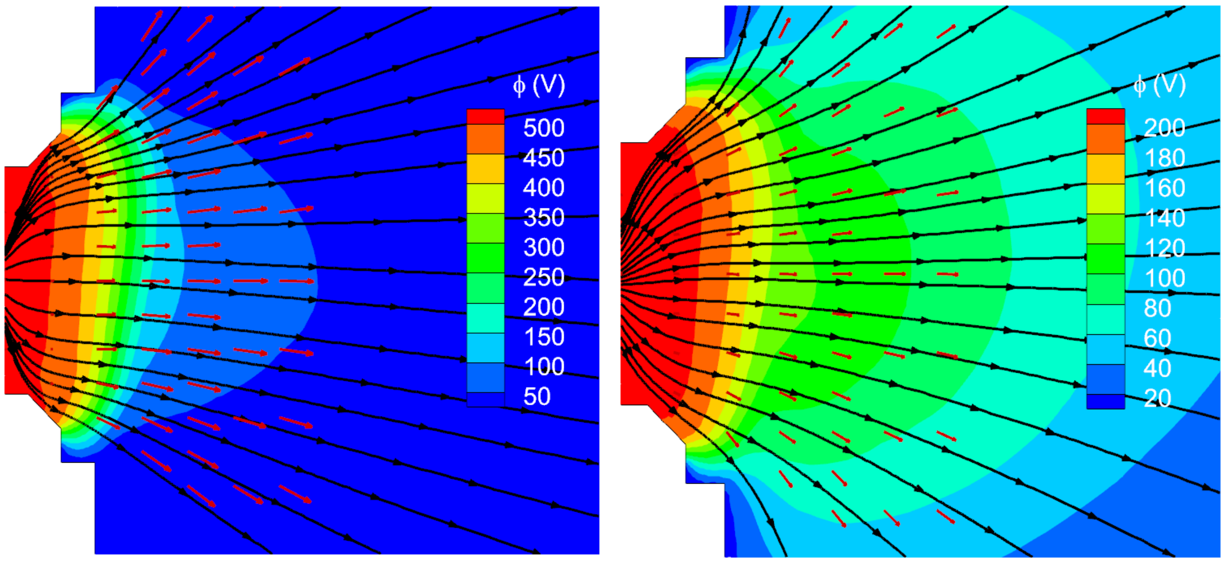

Fig. 4: Ion velocity vectors at the edges of the beam extracted from LIF measurements (red) and superimposed to time-averaged velocity streamtraces obtained from Hall2De simulation for MaSMi at 500 V – 2 A (left) and 200 V – 1 A (right). We found that the simulation results at the intermediate operating condition (400 V – 2 A) displays a similar level of agreement with the measurements.

IV. Erosion rate predictions

A. Comparison with measurements and discussion of results

Erosion rates are computed using the procedure outlined in [25] for the three operating conditions in Table I. We found the erosion rates at the acceleration channel to be negligible (as expected for a magnetic shielded topology) and thus we do not report them in this article. We instead focus on the predictions for the pole covers. One of the advantages of the multi-fluid + PIC algorithm in Hall2De is that it allows us to identify which fluid populations have significant contributions to the erosion. In the case of MaSMi, we found that singly-charged ions from the channel (iF=1, iC=1) and PIC ions produce most of the erosion. Thus, in Fig. 5, we report the total erosion from the simulations along the pole surface and the contributions of iF=1, iC=1 and PIC ions to it. The figures are non-dimensionalized by the distance between the inner and outer diameters of the pole, L_{IFPC} and L_{OFPC}, for the inner and outer poles, respectively, with r/L=0 and r/L=1 at the inner and outer diameters, respectively.

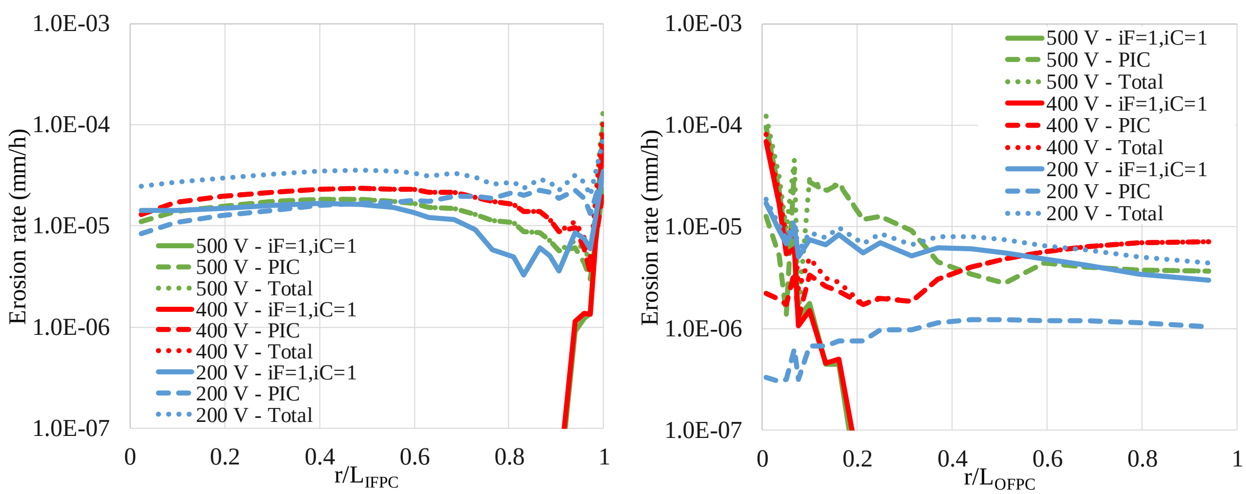

Fig. 5: Erosion rates along the main inner (left) and outer (right) pole surfaces. We show total erosion rates and contributions of beam ions (iF=1, iC=1) and plume ions (PIC)

We find that the results for the 400 and 500 V operating conditions exhibit similar trends. The contribution of beam ions to the erosion is restricted to the edges of the poles that are closer to the discharge channel (r/L_{IFPC}>0.9 and R/L_{OFPC}<0.1, respectively for the inner and outer poles). This contrasts with the H6MS [25], where significant contribution of high energy ions was found everywhere on the pole surface due to a more downstream location of the acceleration region. As can be observed in Fig. 4, the beam ions grace the corner of the outer pole at an approximately 45-degree angle. As a consequence, beam ions only sputter the corner exposed to the beam but cannot be turned around to sputter the main surface of the pole cover. In the H6MS [25] on the contrary, some high energy ions were accelerated at an almost 90-degree angle with respect to the thrust vector. In Fig. 6, we observe that in effect the ion current density of beam ions decreases by multiple orders of magnitude within the first 20% of the pole surface. In Fig. 7, we depict the average ion energy of the ion populations. In the 400 and 500 V cases, the energy of the ions is approximately 150 V lower than the discharge voltage. This indicates that beam ions that can reach the surface of the poles are generated within the acceleration region (i.e., not upstream in the channel) and close to the thruster walls. Ions modeled by PIC are responsible for most of the erosion in regions of the pole surfaces that are further from the channel exit. These ions exhibit an almost constant current density of about 20 A/m^2 with an average energy of 60 V and are generated downstream of the acceleration region. These ions can be turned around towards the pole by the curvature of the plasma potential (see Fig. 4) due to their relatively low energy compared to the beam ions. In MaSMi, the contribution to these ions to the erosion is more significant than in other magnetically shielded thrusters, such as the H6MS [25]. We have found that ionization and charge exchange rates downstream of the acceleration regions are larger than in other modern magnetically shielded thrusters (when thruster dimensions are scaled) as MaSMi exhibits a slightly lower mass efficiency. The latter results in a larger population of neutral atoms in the plume which in turn leads to larger ionization and cross-section rates. For instance, the 500 V – 2 A condition has a mass efficiency of 0.8 while the 300 V condition in HERMeS has a mass efficiency close to 1. We also expect that the sharp increase of erosion rates near the outer diameter of the inner pole and inner diameter of the outer pole will become smoother as the corner erodes and becomes blunt. This phenomenon will allow for beam ions to reach further onto the pole surface but at a lower ion current density than predicted in our simulations at the corner. Thus, we predict that the erosion profile will become smoother with time in the regions r/L_{IFPC}>0.75 and r/L_{OFPC}<0.25.

The predictions for the erosion at 200 V – 1 A exhibit significant differences with the other two cases. At 200 V, the contribution to the beam ions to the erosion extends to the entire pole surface. This is a result of the large oscillations found for this operating condition. During the period of one oscillation, as shown in [28], the divergence of the beam increases for one half-period and decreases for the other half. However, when the beam divergence is large, the trajectories of higher energy ions can intersect the pole surfaces. In Fig. 7, we observe that at 200 V, the average energy of the beam ions is close to the discharge voltage while it was ~150 V below for the 400 and 500 V cases. The energy of the ions modeled with PIC is also larger, which compensates for the lower ion current density of these ions with respect to the 400 and 500 V operating conditions (Fig. 6). A lower current density of ions is expected at 200 V because the discharge current has been reduced by half. These results are similar to those for HERMeS at 600 V [27], where the presence of high-amplitude plasma oscillations also increased the erosion rates with respect to a non-oscillatory case.

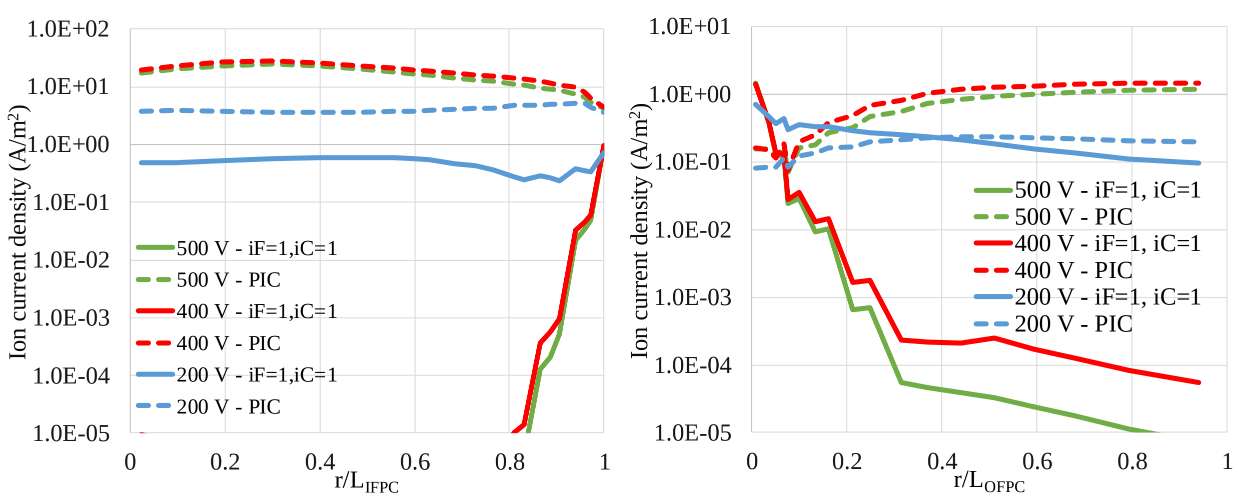

Fig. 6: Ion current density of beam ions (iF=1, iC=1) and plume ions (PIC) along the main inner (left) and outer (right) pole surfaces.

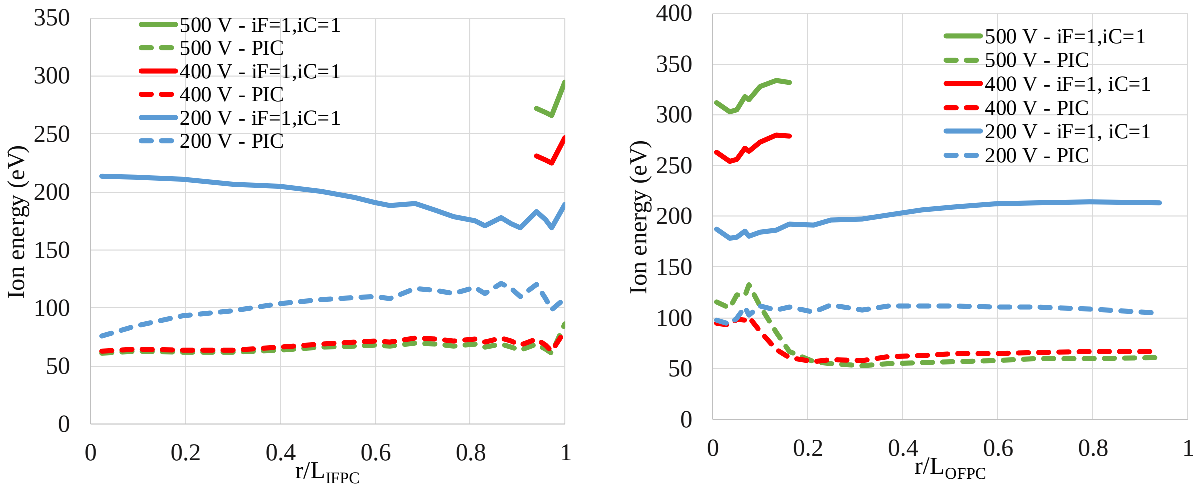

Fig. 7: Average energy of beam ions (iF=1, iC=1) and plume ions (PIC) along the main inner (left) and outer (right) pole surfaces. Ion energy profile for iF=1, iC=1 at 400 and 500 V only showed in regions where the ion current density is non-negligible.

Comparisons of the radial distribution along the pole cover surfaces of the measured erosion rates after short-duration (~200 h) wear tests [29] are depicted in Figs. 8-10. In the wear test, the pole cover surfaces were scanned radially and azimuthally. The results are shown as a function of radial location along the pole with erosion rates averaged in the azimuthal direction. We also depict the measured erosion rates at opposite locations (0 and 180 degrees). Some of the results, especially for the outer pole cover at 400 and 500 V, exhibit large azimuthal asymmetries. For instance, the erosion rates at the 180-degree location for the outer pole cover in the 500 V operating condition are negligible (comparable to the deposition rate, estimated to be 10^{-7} mm/h) while they are more than ten times larger than the deposition rate at the 0-degree location. The measured data also exhibits a non-monotonic profile in certain cases, with multiple local maxima and minima. Explaining the features of the measured profiles is beyond the scope of this article and the reader is referred to [29] for further details on the experimental results. The uncertainty in the measurements [29] was quantified as 8×10^{-6}, 5×10^{-6}, and 4×10^{-6} mm/h for the 500, 400, and 200 V conditions, respectively.

In general, the results are in good agreement with the experimental results when accounting for uncertainties in the measurements (i.e., azimuthal averaging, irregularities in the initial surface) and the model (i.e., uncertainty in the sputtering rate at a given energy, quantified in [25] to be approximately a factor of two for ion energy values below 150 V). At the inner front pole cover, the predictions of the simulations are larger (by less than a factor of two) in the region $r/L_{IFPC}<0.5$ for the three operating conditions. Closer to the outer edge ($r/L_{IFPC}>0.75$), the measured erosion rates exhibit an upward trend that is not followed in the simulations until $r/L_{IFPC}>0.95$. As mentioned in the discussion above, we expect the sharp increase in erosion rates observed in simulation results to become smoother with a blunt corner, leading to better agreement with the measured values for $r/L_{IFPC}>0.75$. The experimental results already reflect a time-averaged erosion rate for the duration of the wear test that includes the effect of a corner that is becoming progressively more rounded. Unfortunately, the measured erosion rates for $r/L_{IFPC}>0.85$, which would quantify how much the corner has eroded, were difficult to analyze [29] and are not presented.

At the outer pole cover, the measured and computed erosion rates are also within a factor of two. We must point out that at the 400 V and 500 V operating conditions, one side of the pole cover appears to have almost negligible erosion so the best comparison possible is with the azimuthally averaged profile. At 200 V – 1 A, the simulation consistently underpredicts the measurement (which exhibits a lower degree of azimuthal variation). The latter can be due to the fact that the large oscillations that drive the increase in erosion rates at 200 V – 1 A were produced by imposing a sinusoidal change in the anomalous collision frequency (Section III). As the physics of the acceleration region remain unclear, the approximation employed in our model may not be completely accurate.

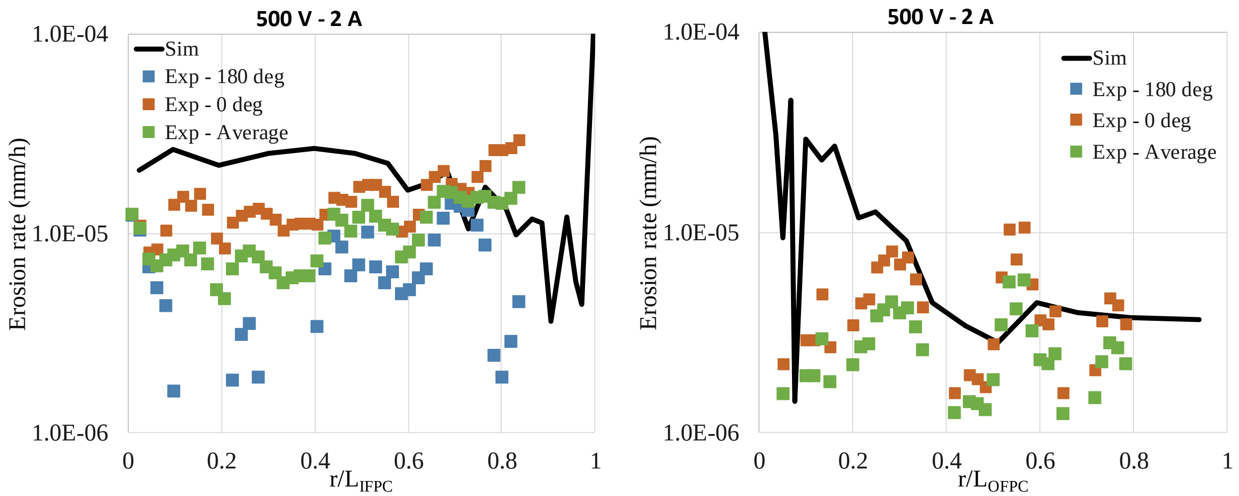

Fig. 8: Comparison between numerical predictions and wear test results for the erosion rate at the inner (left) and outer (right) front pole cover at 500 V – 2 A. Uncertainty in the measurement [29] is $8\text{x}10^{-6}$ mm/h.

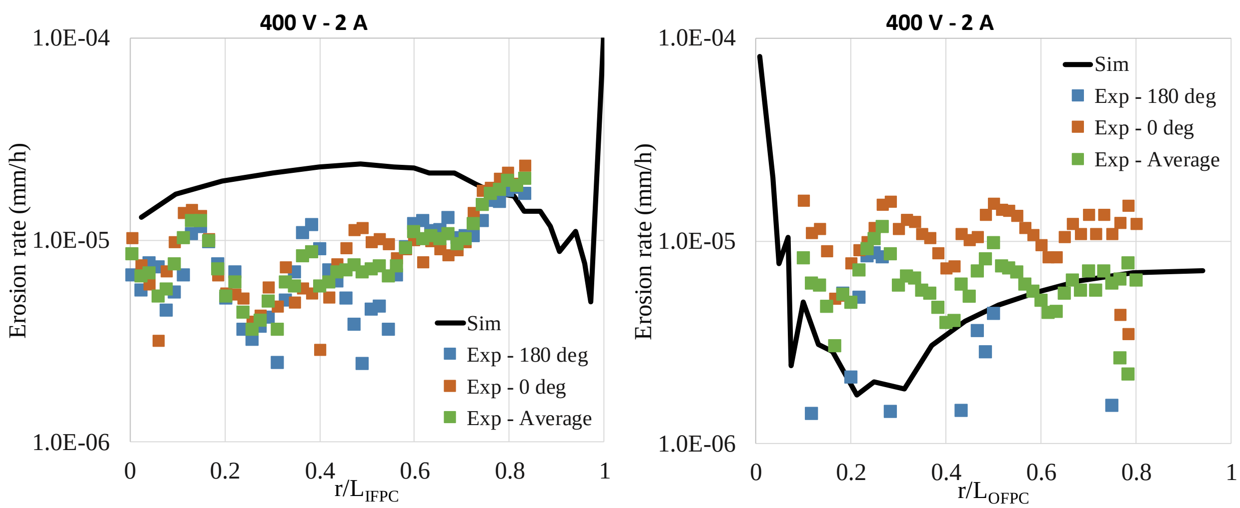

Fig. 9: Comparison between numerical predictions and wear test results for the erosion rate at the inner and outer front pole cover at 400 V – 2 A. Uncertainty in the measurement [29] is $5\text{x}10^{-6}$ mm/h.

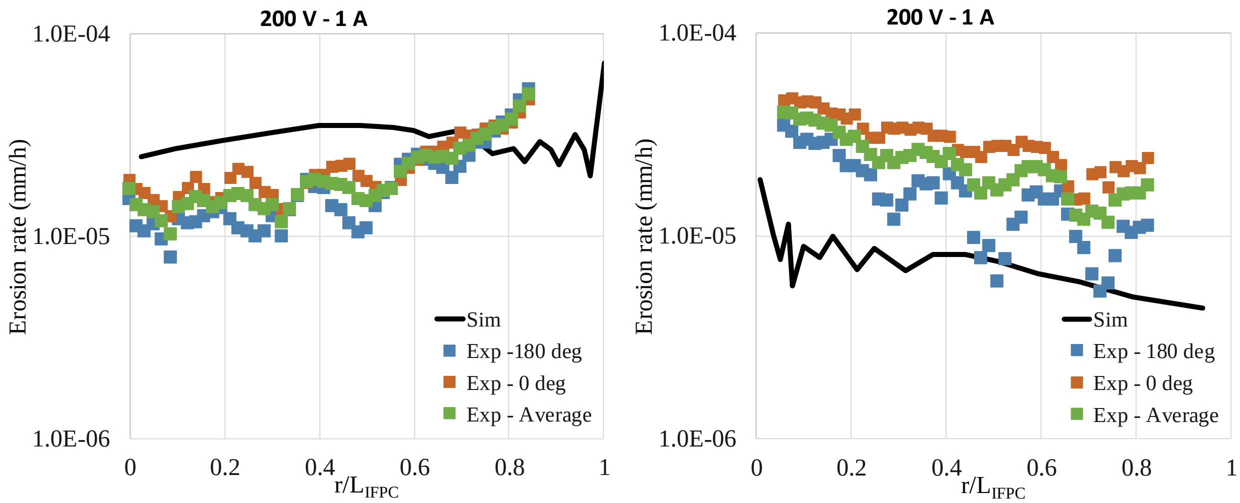

Fig. 10: Comparison between numerical predictions and wear test results for the erosion rate at the inner and outer front pole cover at 200 V – 1 A. Uncertainty in the measurement [29] is 4x10^{-6} mm/h.

Finally, we report on the erosion rates at the outer diameter of the inner pole cover and inner diameter of the outer pole cover. These surfaces are parallel to the channel centerline and, thus, more exposed to sputtering by beam ions. In Table II, we summarize the total erosion rate and the average energy and current density of the ions that produce it. The contribution of ions modeled by PIC is not relevant in these surfaces and most of the erosion comes from singly charged beam ions (iF=1, iC=1). We observe that the erosion rates at these lateral surfaces are larger than at the maximum erosion rates predicted at the front surfaces (at r/L_{IFPC} = 1 and r/L_{OFPC} = 0, for the inner and outer pole covers respectively) by approximately a factor of 2 and an order of magnitude larger than the values found at the midpoint of the front surfaces. As the lateral surfaces exposed to the beam erode at a larger rate than the front surfaces, we expect the edges of the pole cover to become curved. This effect in principle will expose more of the front surface of the pole to the beam ions, the net result being that the sharp drop in the beam ion current density observed at r/L_{IFPC}>0.9 and R/L_{OFPC}<0.1 will become more gradual and extend further in distance from the edge of the front surface.

Table II. Erosion rates at outer diameter of IFPC and inner diameter of OFPC facing the discharge channel

Operating condition	IFPC ion energy (eV)	IFPC ion current density (A/m^2)	IFPC erosion rate (mm/h) x10^{-6}	OFPC ion energy (eV)	OFPC ion current density (A/m^2)	OFPC erosion rate (mm/h) x10^{-6}
500 V – 2 A	405	2.31	155.4	410	5.35	208.1
400 V – 2 A	350	4.38	137.4	321	7.17	197.2
200 V – 1 A	182	5.29	54.2	193	4.59	47.3

B. Lifetime considerations for ASTRAEUS

The requirements for ASTRAEUS call for a total xenon throughput of 100 kg. The latter will require operation for approximately 10,000 h and 20,000 h at the 500-V and 200-V mass flow rates, respectively. The pole covers have been designed with a thickness of 1.5 mm, which allows for a maximum erosion rate of 150x10^{-6} mm/h or 75x10^{-6} mm/h if the total throughput was performed at 500 or 200 V, respectively. Based on our predictions, the only regions that are prone to be completely eroded at the end of the lifetime of the system are close to the outer diameter of the inner pole cover and the inner diameter of the outer pole cover. As future work, it will be necessary to perform a study by numerical simulation (similar to that presented in [43] for the SPT-140) of the progressive erosion of the pole surface. This will consist of a series of simulations in which the predicted erosion rates are used to define a geometry of the thruster after a fraction of the mission lifetime. The new geometry is then employed to compute updated erosion rates until the end-of-life geometry is reached. This will confirm whether the hypothesis discussed previously that the erosion rates at the corners decrease as they become blunt is correct.

A final consideration is the existence of the pole cover fasteners that are used to attach the pole cover to the thruster and whose surface are exposed to the plasma unless masked. Both Molybdenum and Inconel were considered for these fasteners; the latter of which has an estimated sputtering yield that is at least an order of magnitude larger than graphite for the range of ion energies that are dominant at the midpoint of the pole surfaces (~60 V for 500 V and ~100 V for 200 V) [44]. If the reported erosion rates for a graphite surface in Fig. 5 are multiplied by ten, they exceed the maximum allowable erosion rate to fulfill the system requirements. It is likely that as the Inconel erodes at a faster rate than the rest of the surface, the recessed fastener will be shielded by the pole cover. An updated pole cover has been proposed with the aim of protecting the pole cover fastener. This design features a wedge (Fig. 11), making the pole cover thicker next to the acceleration channel and returning to the nominal thickness at the location of the fastener.

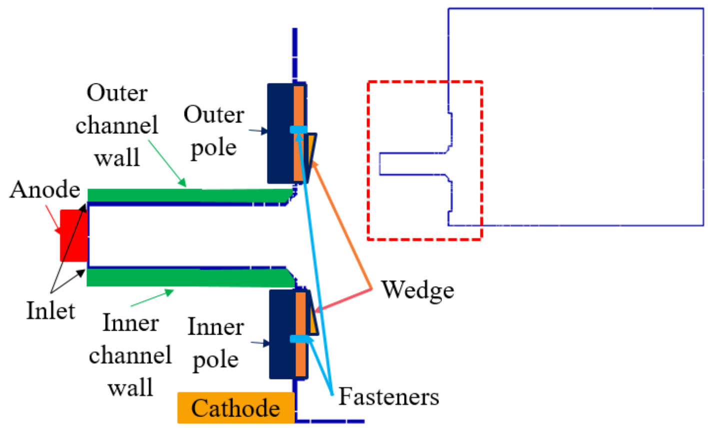

Fig. 11: MaSMi schematic with updated pole cover design featuring wedge to shield Inconel fasteners

Figure 12 depicts the ion current density of ions sputtering the inner pole cover for the 500 V – 2 A operating condition with and without the wedge. We observe that the new geometry reduces the ion current density at the downstream portion of the surface by factors of 2 to 2.5. As shown in Fig. 6, plume ions modeled with PIC dominate this region. The average energy of these ions is also slightly reduced as the wedge mostly blocks ions coming from nearby the channel exit, where the plasma potential is higher (see Fig. 4). In Fig. 12, we also plot the radial profile of the erosion rate on the new geometry, accounting for the change of material at the location of the fastener. The simulations with a flat surface do not account for the presence of the fastener. At the surface of the wedge, the erosion rates are comparable to those found in the simulations with a flat pole cover. This is expected as the current density of ions does not change significantly since the wedge angle is small. The erosion rate for the Inconel fastener is approximately $100\text{x}10^{-6}$ mm/h, which is 2 times lower than the expected erosion rate on a flat pole cover surface. Table III summarizes the computed erosion rates for the Inconel fasteners at the three operating conditions described in Table I. The presence of the wedge in principle reduces the erosion rate of the fasteners below the requirement of $150\text{x}10^{-6}$ mm/h for the 400 and 500 V operating conditions. The 200 V – 1 A has a more stringent requirement due to the lower mass flow rate (~$75\text{x}10^{-6}$ mm/h) which is not met even with the addition of the wedge. It is also likely that the wedge will become less effective with time as it erodes faster than the region of the pole cover that is shielded. This phenomenon can be assessed by performing a series of simulations in which the surfaces of the thruster are progressively eroded. It is unlikely though that a mission profile would require continuous thrusting at the 200 V – 1 A condition so lifetime predictions will have to be tailored to specific mission profiles based on these results. A graphite mask on top of the pole cover fasteners is presently being considered in the thruster design space to completely eliminate the risk of fastener erosion.

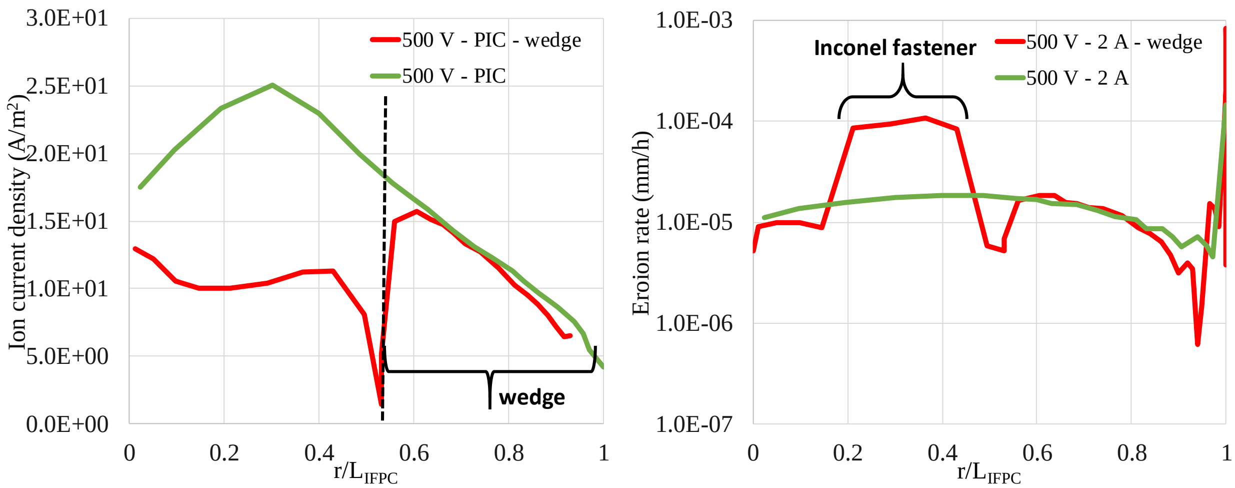

Fig. 12. Left: Radial profile of ion current density of plume ions modeled with PIC along the inner pole cover with wedge compared to the profile for a flat surface cover (Fig. 6) for the 500 V- 2 A operating condition. Right: radial profile of erosion rates along the inner pole cover with wedge compared to the profile for a flat surface cover (Fig. 5). The profile for the flat surface does not account for the presence of the Inconel fastener (i.e., assumes the whole surface is made of graphite)

Table III. Comparison between computed erosion rates for Inconel fastener with wedge geometry and flat geometry

Erosion rate Inconel ($x10^{-6}$ mm/h)	Wedge inner pole cover	Flat inner pole cover	Wedge outer pole cover	Flat outer pole cover
500 V – 2 A	101.2	195.3	10.2	23.4
400 V – 2 A	110.7	230.5	14.8	31.1
200 V – 1 A	158.2	385.2	51.2	115.3

V. Conclusion

ASTRAEUS is an in-space propulsion technology that is being developed with the aim of enabling high delta-V interplanetary exploration using SmallSats and features a magnetically shielded miniature (MaSMi) Hall thruster. Erosion of the magnetic poles of magnetically shielded thrusters has been identified in the past as a potential life-limiting mechanism that can be prevented by installing a thin cover a few millimeters thick made of a material with low sputtering yield such as graphite. We conducted numerical simulations, using the 2-D axisymmetric code Hall2De, to predict whether the proposed cover, with a thickness of 1.5 mm, erodes completely before the xenon throughput outlined in the ASTRAEUS requirements (100 kg) can be completed. At a discharge current of 2 A, the throughput requirement is achieved after 10,000 h of operation while it takes double that time with a discharge current of 1 A.

We considered three operating conditions representative of the MaSMi operating envelope (500 V – 2 A, 400 V – 2 A, and 200 V – 1 A). The numerical simulations were informed by direct measurements of the plasma conditions in the acceleration channel that were obtained using LIF diagnostics. For the 500- and 400-V operating conditions, plasma oscillations are small and the erosion of the poles is driven by ions of moderate energy (approximately 50 to 150 V) generated downstream of the acceleration region. The only regions that are sputtered by higher energy ions are those exposed directly to the beam ions: the outer diameter of the inner pole cover and the inner diameter of the outer pole cover. The erosion rates at these locations are higher, being close to the maximum erosion rate ($150x10^{-6}$ mm/h) allowed by the throughput requirements. For the 200 V - 1 A operating condition, the erosion rates along the front surface of the poles are increased due to the presence of large plasma oscillations. However, they are below, by a factor of 0.5, of the maximum allowable erosion rate at this condition ($75x10^{-6}$ mm/h). At the corners exposed to the beam ions, the erosion rates are not as large as those found at 400 – 2 A and 500 V – 2 A as the density of beam ions is lower. However, they are still larger than at locations of the surface further from the acceleration channel and only slightly below the maximum allowable erosion rate. We hypothesize that as the corners erode and become blunt, the erosion rate will decrease and become more evenly distributed along the pole surface, contrary to the sharp increase near the corner observed in the erosion predictions based on these beginning-of-life simulations. As future work, we may need to conduct a series of simulations in which the surface of the pole cover is progressively eroded until it reaches the end-of-life condition.

We finally investigated an updated cover surface geometry that features a wedge. This wedge aims at shielding the pole cover fasteners that attach the cover to the thruster. Inconel has a sputtering yield that is more than an order of magnitude higher than the graphite material employed for the pole cover at the typical energies of ions sputtering the pole surface. We found that the wedge is effective at shielding the fastener, decreasing the ion current density by factors of 2 to 3. While the predicted erosion rates for the Inconel fasteners were above the maximum allowable erosion rate with a flat surface, the inclusion of the wedge is sufficient to lower the erosion rates to acceptable values for the 400- and 500-V operating conditions but not for the 200 V – 1 A operating condition. However, it is unlikely that a mission profile will feature continuous operation at the latter. The effectiveness of the wedge with time must also be investigated with a series of simulations in which the thruster surfaces are progressively eroded. Fully masking all of the pole cover fasteners with graphite is currently being investigated to fully mitigate pole cover fastener erosion.

Acknowledgments

This research was carried out at the Jet Propulsion Laboratory, California Institute of Technology, under a contract with the National Aeronautics and Space Administration and funded through the internal Research and Technology Development program.

References

[1] Conversano, R. W., Barchowsky, A., Lobbia, R. B., Chaplin, V. H., Lopez Ortega, A., Lui, A. D., Loveland, J. A., Goebel, D. M., Snyder, J. S., Hofer, R. R., Carr, G. A., Randolph, T. M., "Overview of the Ascendant Sub-kW Transcelestial Electric Propulsion System", IEPC-2019-282, 36th International Electric Propulsion Conference, Vienna, Austria, September 2019

[2] Sutin, B. M., Cutts, J., Didion, A. M., Drilleau, M., Helbert, J., Karp, A., Kenda, B., Komjathy, A., Krishnamoorthy, S., Lantoine, G., Lognonné, P., Makela, J., Nakazono, B., Rud, M., and Wallace, M., "VAMOS : a SmallSat mission concept seismic activity from orbit," *SPIE, Journal of International Society for Optics and Photonics*, Jul. 2018, DOI: 10.1117/12.2309439.

[3] Woolley, R., and Olikara, Z., "Optimized Low-Thrust Missions from GTO to Mars," *2019 IEEE Aerospace Conference*, Big Sky, MT: 2019.

[4] Conversano, R. W., Rabinovitch, J., Strange, N. J., Arora, N., Jens, E., and Karp, A. C., "SmallSat Missions Enabled by Paired Low-Thrust Hybrid Rocket and Low-Power Long-Life Hall Thruster," *2019 IEEE Aerospace Conference*, Big Sky, MT: 2019

[5] Conversano, R. W., Goebel, D. M., Hofer, R. R., Matlock, T. S., and Wirz, R. E., "Development and Initial Testing of a Magnetically Shielded Miniature Hall Thruster," *IEEE Transactions on Plasma Science*, 1, vol. 43, 2015, DOI: 10.1109/TPS.2014.2321107.

[6] Conversano, R. W., Arora, N., Goebel, D. M., and Wirz, R. E., "Preliminary Mission Capabilities Assessment of a Magnetically Shielded Miniature Hall Thruster," *65th IAF/IAA/IISL International Astronaturical Congress*, IAC-14.C4.4.4, Toronto, Canada: 2014.

[7] Conversano, R. W., Goebel, D. M., Mikellides, I. G., Hofer, R. R., Matlock, T. S., and Wirz, R. E., "Magnetically Shielded Miniature Hall Thruster: Performance Assessment and Status Update," *50th AIAA Joint Propulsion Conference*, AIAA-2014-3896, Cleveland, OH: 2014.

[8] Conversano, R. W., Goebel, D. M., Hofer, R. R., Mikellides, I. G., Katz, I., and Wirz, R. E., "Magnetically Shielded Miniature Hall Thruster: Design Improvement and Performance Analysis," *34th ERPS International Electric Propulsion Conference*, IEPC-2015-100 / ISTS-2015-b-100, Kobe, Japan: 2015.

[9] Conversano, R. W., "Low-Power Magnetically Shielded Hall Thrusters," Ph.D. Thesis, Department of Mechanical and Aerospace Engineering, University of California, Los Angeles, 2015.

[10] Conversano, R. W., Arora, N., Strange, N. J., and Goebel, D. M., "An Enabling Low-Power Magnetically Shielded Hall Thruster for Interplanetary Smallsat Missions," *Interplanetary Small Satellite Conference*, Pasadena, CA: 2016.

[11] Conversano, R. W., Goebel, D. M., Hofer, R. R., and Arora, N., "Performance enhancement of a long-life, low-power hall thruster for deep-space smallsats," *IEEE Aerospace Conference*, Big Sky, MT: 2017.

[12] Conversano, R. W., Goebel, D. M., Hofer, R. R., Mikellides, I. G., and Wirz, R. E., "Performance analysis of a low-power magnetically shielded hall thruster: Experiments," *Journal of Propulsion and Power*, 4, vol. 33, 2017, DOI: 10.2514/1.B36230.

[13] Conversano, R. W., Goebel, D. M., Mikellides, I. G., Hofer, R. R., and Wirz, R. E., "Performance analysis of a low-power magnetically shielded hall thruster: Computational modeling," *Journal of Propulsion and Power*, 4, vol. 33, 2017, DOI: 10.2514/1.B36231.

[14] Conversano, R. W., Lobbia, R. B., Tilley, K. C., Goebel, D. M., Reilly, S., Mikellides, I. G., and Hofer, R. R., "Development and Initial Performance Testing of a Low-Power Magnetically Shielded Hall Thruster with an Internally-Mounted Hollow Cathode," *35th International Electric Propulsion Conference*, IEPC-2017-64, Atlanta, GA: 2017.

[15] Conversano, R. W., Lobbia, R. B., Kerber, T. V., Tilley, K. C., Goebel, D. M., Reilly, S. W., Mikellides, I. G., and Hofer, R. R., "Performance Characterization of a Low-Power Magnetically Shielded Hall Thruster with an Internally-Mounted Hollow Cathode," *Plasma Sources Science and Technology*, 2019.

[16] Mikellides, I. G., Katz, I., Hofer, R. R., Goebel, D. M., de Grys, K., and Mathers, A., "Magnetic Shielding of the Channel Walls in a Hall Plasma Accelerator", Physics of Plasmas, Vol. 18, 033501, 2011, doi:10.1063/1.3551583

[17] Hofer, R. R., Kamhawi, H., Herman, D., Polk, J. E., Snyder, J. S., Mikellides, I., Huang, W., Myers, J., Yim, J., Williams, G., Lopez Ortega, A., Jorns, B., Sekerak, M., Griffiths, C., Shastry, R., Haag, T., Verhey, T., Gilliam, B., Katz, I., Goebel, D. M., Anderson, J. R., Gilland, J., and Clayman, L., "Development Approach and Status of the 12.5 kW HERMeS Hall Thruster for the Solar Electric Propulsion Technology Demonstration Mission," *34th International Electric Propulsion Conference*, IEPC-2015-186, Kobe, Japan: 2015.

[18] Hofer, R., Polk, J., Sekerak, M., Mikellides, I., Kamhawi, H., Verhey, T., Herman, D., and Williams, G., "Development Status of the 12.5 kW HERMeS Hall Thruster for the Solar Electric Propulsion Technology Demosntration Mission," *52nd AIAA Joint Propulsion Conference*, AIAA-2016-4825, Salt Lake City, UT: 2016.

[19] Hofer, R., Polk, J. E., Mikellides, I. G., Lopez Ortega, A., Conversano, R. W., Chaplin, V. H., Lobbia, R. B., Goebel, D. M., Kamhawi, H., Verhey, T., Williams, G., Mackey, J., Huang, W., Yim, J., Herman, D. A., and Peterson, P. Y., "Development Status of the 12.5 kW Hall Effect Rocket with Magnetic Shielding (HERMeS)," *35th International Electric Propulsion Conference*, IEPC-2017-231, Atlanta, GA: 2017.

[20] K. De Grys, A. Mathers, and B. Welander, "Demonstration of 10,400 hours of operation on a 4.5kW qualification model Hall thruster," in Proceedings of the 46th AIAA/ASME/SAE/ASEE Joint Propulsion Conference, Nashville, TN, AIAA Paper 2010-6698, 2010.

[21] Mikellides, I.G., Katz, I, Hofer, R.R, and Goebel, D. M., "Magnetic Shielding of a Laboratory Hall Thruster, I, Theory and Validation", Journal of Applied Physics, Vol. 115, 043303, 2014, doi: 10.1063/1.4862313

[22] Hofer, R. R., Goebel, D. M., Mikellides, I. G., and Katz, I., "Magnetic Shielding of a Laboratory Hall Thruster, II, Experiments", Journal of Applied Physics, Vol. 115, 043304, 2014, doi:10.1063/1.4862314

[23] Haas, J. M., Hofer, R. R., Brown, D. L., B, Reid, B. M., and Gallimore, A. D., "Design of a 6-kW Hall thruster for high thrust/power investigation", in 54th JANNAF Propulsion Meeting, Denver, Colorado, 2007.

[24] Sekerak, J. M., Hofer, R. R., Polk, J. E., Jorns, B. A., and Mikellides, I. G., "Wear Testing of a Magnetically Shielded Hall Thruster at 2000-s Specific Impulse", IEPC 2015-155, July 2015.

[25] Lopez Ortega, A, Mikellides, I. G., Sekerak, M. J, and Jorns, B. A., "Plasma Simulations in 2-D (r-z) Geometry for the Assessment of Pole Erosion in a Magnetically Shielded Hall Thruster", Journal of Applied Physics, Vol. 125, 033302, 2019, doi:10.1063/1.5077097

[26] Williams, G., Gilland, J. H., Kamhawi, H., Choi, M., Peterson, P. Y., and Herman, D., "Wear Trends of the HERMeS Thruster as a Function of Throttle Point," IEPC-2017-207, October 2017.

[27] Lopez Ortega, A., Mikellides, I. G., and Chaplin, V. H., "Numerical Simulations for the Assessment of Erosion in the 12.5-kW Hall Effect Rocket with Magnetic Shielding", IEPC 2017-154, 35th International Electric Propulsion Conference, Atlanta, GA, October 2017

[28] Lopez Ortega, A., Mikellides, I. G., and Katz, I., "Hall2De Numerical Simulations for the Assessment of Pole Erosion in a Magnetically Shielded Hall Thruster", IEPC 2015-249, July 2015.

[29] Lobbia, R. B., et al., "Pole Erosion Measurements for the Development Model of the Magnetically Shielded Miniature Hall Thruster", IEPC 2019-298

[30] Mikellides, I. G. and Katz, I., "Numerical Simulations of Hall-effect Plasma Accelerators on a Magnetic-Field-Aligned Mesh", Physical Review E, Vol. 86, 2012, p. 046703, doi: 10.1103/PhysRevE.86.046703

[31] Lopez Ortega, A. and Mikellides, I. G., "The Importance of the Cathode Plume and its Interactions with the Ion Beam in Numerical Simulations of Hall Thrusters", *Physics of Plasmas*, Vol. 23, 043515, 2016, doi: 10.1063/1.4947554

[32] Katz, I. and Mikellides, I. G., "Neutral gas free molecular flow algorithm including ionization and walls for use in plasma simulations", *Journal of Computational Physics*, Vol. 230, 2011, pp. 1454-1464, doi: 10.1016/j.jcp.2010.11.013

[33] Hobbs, G. D., and Wesson, J. A., "Heat Flow through a Langmuir Sheath in Presence of Electron Emission," *Plasma Physics*, vol. 9, no. 1, pp. 85-87, 1967, doi: 10.1088/0032-1028/9/1/410

[34] Doerner, R. P., Whyte, D. G., and Goebel, D. M., "Sputtering Yield Measurements during Low Energy Xenon Plasma Bombardment", *Journal of Applied Physics*, Vol. 93, No. 9, 2003, pp. 5816, doi: 10.1063/1.1566474

[35] Rosenberg, D., and Wehner, G. K., "Sputterin Yields for Low Energy He+-,Kr+-, and Xe+-Ion Bombardment", Journal of Applied Physics, Vol. 33, pp. 1842, 1962, doi:10.1063/1.1728843

[36] Kolasinski, R. D., Polk, J. E., Goebel, D. M., and Johnson, L. K., "Carbon Sputtering Yield Measurements at Grazing Incidence", Applied Surface Science, Vol. 254, 8, pp.2506-2515, 2007, doi:101.016/j.apsusc.2007.09.082

[37] Cedolin, R. J., Hargus, W. A., Storm, P. V, Hanson, R. K., and Cappelli, M. A., "Laser-Induced Fluorescence Study of a Xenon Hall Thruster", Applied Physics B, Vol. 65, Issue 4-5, pp. 459-469, 1997, doi: 10.1007/s003400050297

[38] Hargus, W. A., and Cappelli, M. A., "Laser-Induced Fluorescence Measurements of Velocity within a Hall Discharge", *Applied Physics B*, Vol. 72, Issue 8, pp 961-969, 2001, doi: 10.1007/s003400100589

[39] Chaplin, V. H., et al., "Ion Velocity Measurements in the Magnetically Shielded Miniature Hall Thruster (MaSMi) Using Laser-Induced Flourescence", IEPC 2019-531
[40] Heron, A., and Adam, J. C., "Anomalous Conductivity in Hall Thrusters: Effects of the Non-linear Coupling of the Electron-Cyclotron Drift Instability with Secondary Electron Emission of the Walls", Physics of Plasmas, Vol. 20, 082313, 2013, doi: 10.1063/1.4818796
[41] Adam, J. C., Heron, A., and Laval, G., "Study of Stationary Plasma Thrusters Using Two-dimensional Fully Kinetic Simulations", Physics of Plasmas, Vol. 11, 2004, 295, doi: 10.1063/1.1632904
[42] Dale, E. T., and Jorns, B. A., "Non-invasive Time-Resolved Measurements of Anomalous Collision Frequency in a Hall Thruster", Physics of Plasmas, Vol. 26, 013516, 2019, doi:10.1063/1.5077008
[43] Lopez Ortega, A., Mikellides, I. G., Chaplin, V. H., Snyder, J. S., Lenguito, G., "Numerical Investigations of Background Pressure Effects and Channel Erosion in the SPT-140 Hall Thruster for the Psyche Mission, IEPC 2019-263
[44] Zhou, X. W., Wadley, H. N. G., and Sainathan, S., "Low Energy Sputtering of Nickel by Normally Incident Xenon Ions", Nuclear Instruments and Methods in Physics Research B: Beam Interactions with Materials and Atom, Vol. 234, Issue 4, 2005, 441-457, doi: 10.1016/j.nimb.2005.02.016